ChemPhotoChem

Research Article
doi.org/10.1002/cptc.202300212

Chemistry Europe
European Chemical Societies Publishing

www.chemphotochem.org

Near-Infrared Emissive Indolizine Squaraine Fluorophores as Strong Molecular Viscosity Sensors

David Ndaleh[+],[a] William E. Meador[+],[a] Cameron Smith,[a] Hannah C. Friedman,[b] Madison McGuire,[a] Justin R. Caram,[b] Nathan I. Hammer,[a] and Jared H. Delcamp*[a, c]

Changes in the viscosity of intracellular microenvironments may indicate the onset of diseases like diabetes, blood-based illnesses, hypertension, and Alzheimer's. To date, monitoring viscosity changes in the intracellular environment remains a challenge with prior work focusing primarily on visible light-absorbing viscosity sensing fluorophores. Herein, a series of near-infrared (NIR, 700–1000 nm) absorbing and emitting indolizine squaraine fluorophores (**1PhSQ**, **2PhSQ**, **SO_3SQ**, **1DMASQ**, **7DMASQ**, and **1,7DMASQ**) are synthesized and studied for NIR viscosity sensitivity. **2PhSQ** exhibits a very high slope in its Forster-Hoffmann plot at 0.75 which indicates this dye is a potent viscosity sensor. The properties of the squaraine fluorophores are studied computationally *via* density functional theory (DFT) and time-dependent (TD)-DFT. Experimentally, both steady-state and time-resolved emission spectroscopy, absorption spectroscopy, and electrochemical characterization are conducted on the dyes. Precise photophysical tuning is observed within the series with emission maxima wavelengths as long as 881 nm for **1,7DMASQ** and fluorescence quantum yields as high as 39.5 and 72.0% for **1PhSQ** in DCM and THF, respectively. The high tunability of this molecular scaffold renders indolizine squaraine fluorophores excellent prospects as viscosity-sensitive biological imaging agents with **2PhSQ** giving a dramatically higher fluorescence quantum yield (from 0.3 to 37.1%) as viscosity increases.

Introduction

Changes in the viscosity of intracellular microenvironments can signify a chemical imbalance that can indicate the onset of diseases including cancer,[1] Alzheimer's,[2] blood-based illnesses,[3] diabetes, hypertension, atherosclerosis,[4] and shear stress in blood vessels.[5] Monitoring early change in the viscosity of cellular microenvironments could be key to early diagnosis of these diseases, and provide guides to possible cures.[1,6] However, due to the complex nature of biological matrices, it is still a challenge of how to best map viscosity changes in cellular microenvironments.[7] Additionally, in the chemical industry, viscosity analysis is routinely employed to ensure consistency in the production and transportation of fluid media.[8] Thus, a viscosity sensitive dye capable of monitoring microenvironments could have a significant impact in both biological and chemical applications.

Fluorescence-based viscosity sensors are materials that exhibit a positive relationship between their fluorescence quantum yield (Φ_F) and the local viscosity of the surrounding environment.[5b,7] These materials provide a logical means to monitor changes in the viscosity of the cellular microenvironment *via* facile fluorescence-based measurements. Recent progress has been made on the use of organic dyes for studying the viscosity of microenvironments.[9] A series of BODIPY derivatives was recently shown to exhibit high viscosity sensitivity. Among the dye series, ***p*-BP** demonstrated one of the highest viscosity sensitivities in the literature and is used as a reference herein (Figure 1).[10]

Viscosity enhanced fluorescence is often rationalized by the tendency of fluorescence-based viscosity sensors to nonradiatively relax *via* vibrational pathways, exhibiting short photo-

[a] *Dr. D. Ndaleh,[+] Dr. W. E. Meador,[+] Dr. C. Smith, M. McGuire, Prof. N. I. Hammer, Prof. J. H. Delcamp*
Department of Chemistry and Biochemistry
University of Mississippi
University, MS, 38677 (USA)
E-mail: delcamp@olemiss.edu

[b] *Dr. H. C. Friedman, Prof. J. R. Caram*
Department of Chemistry and Biochemistry
University of California Los Angeles
Los Angeles, CA, 90095 (USA)

[c] *Prof. J. H. Delcamp*
Air Force Research Labs
Materials and Manufacturing Directorate (RXNC)
2230 Tenth Street B655, Wright-Patterson AFB, OH 45433 (USA)

[+] *Indicates authors contributed equally*

Supporting information for this article is available on the WWW under https://doi.org/10.1002/cptc.202300212

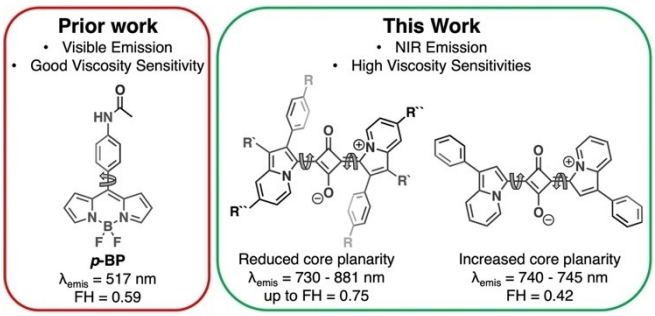

Figure 1. Structures of ***p*-BP** and indolizine squaraine dyes studied herein along with the emission maxima wavelengths (λ_{emis}) and the slope of their respective Forster-Hoffman plots (FH) showing viscosity sensitivity.

luminescent lifetimes, and low Φ_F, when photoexcited in low-viscosity environments.[11] However, in highly viscous environments, restriction of molecular motion reduces the opportunity for vibrational relaxation and increases the likelihood for radiative relaxation *via* fluorescence. Several fluorescence-based viscosity sensors have been developed in recent years by designing molecular systems with strategically placed rotatable groups.[5b,12] However, to date these fluorescence-based viscosity sensors have been largely limited to the visible-light emitters and few examples emit in the near-infrared (NIR, 700–1000 nm).[7,9f] NIR light is more attractive for *in vivo* imaging applications compared to visible light due to deeper tissue penetration, decreased tissue autofluorescence, and lower scattering coefficients that all contribute to the greater signal-to-noise and resolution of *in vivo* images in the NIR.[13] Therefore, there is a need for NIR fluorophores that exhibit high viscosity sensitivity for *in vivo* viscosity tracking.

Squaraine-based fluorophores offer several advantages as candidates for NIR fluorescence-based viscosity sensors owing to their NIR absorption and emission, high photostability, high molar absorptivity (ε), and characteristically high fluorescence quantum yield (Φ_F).[14] Squaraine dyes are composed of two donor groups conjugated through a central four-membered diketo-ring.[14–15] Herein, a series of NIR absorbing and emitting indolizine donor-based squaraine dyes are developed and their viscosity sensitivity probed. Motivated by an exceptionally high Φ_F of 64.9% previously observed for a water soluble indolizine squaraine, **SO_3SQ**, in human serum, the Φ_F of several indolizine donor-based squaraine dyes is studied herein to determine if the increase in Φ_F is viscosity dependent (Figure 2).[16] The use of indolizine heterocycles as donors in place of alkyl amine or indole-based donors is known to induce bathochromic shifts in the absorption and emission of squaraine fluorophores due to an increase in donation strength of the indolizine heterocycle.[17] Herein, the donation strength of the indolizine heterocycle donors are further increased *via* the incorporation of auxiliary *N*,*N*-dimethylaniline (DMA) donors on the indolizine heterocycle, a strategy employed previously with indolizine cyanine dyes.[18]

Results and Discussion

Fluorophore Design

Indolizine squaraine derivatives with variable substituents on the phenyl ring at the 2-position of the indolizine heterocycle have been previously explored and observed to demonstrate minimal tuning of the absorption and emission maxima of the fluorophores.[19] Density functional theory (DFT) computational analysis of the highest occupied molecular orbital (HOMO) of the indolizine squaraine dye demonstrates that the largest HOMO orbital presence is on the 1 and 7 positions of the heterocycle (Figure 2). We hypothesized that substitution of DMA groups at these positions on the indolizine donor would have the largest effect on the donation strength and induce the greatest bathochromic shifts in the absorption and emission maxima. To test this hypothesis, three new derivatives of **2PhSQ** are designed with DMA functionalization at carbon 1 (**1DMASQ**), carbon 7 (**7DMASQ**), and both carbons 1 and 7 (**1,7DMASQ**, Figure 2). Additionally, removal of the phenyl group of **2PhSQ** at carbon 2 of the indolizine donor and relocation to carbon 1 yielded a new fluorophore (**1PhSQ**) for probing the effect of increased planarity through the reduction of steric interactions.

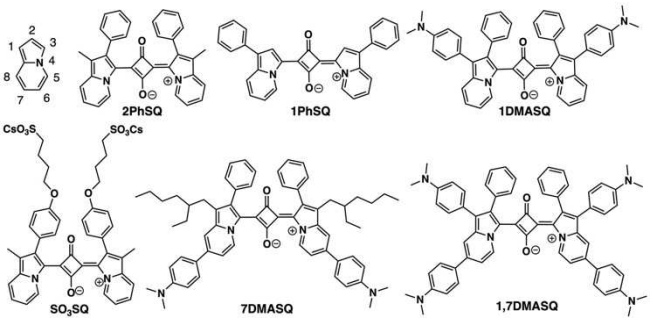

Figure 2. Structures of indolizine, **2PhSQ**, **1PhSQ**, **1DMASQ**, **SO_3SQ**, **7DMASQ**, and **1,7DMASQ**.

Computational Data

Ground-state DFT calculations at the B3LYP/6-311G(*d*,*p*) level of theory and time-dependent (TD)-DFT calculations on the squaraine fluorophores were conducted to determine how the HOMO and lowest unoccupied molecular orbital (LUMO) orbitals contributing to the lowest energy excitation are distributed across the π-system of the fluorophore (Figure 3, Table S1). All derivatives demonstrate 98–100% HOMO to LUMO contribution in their respective lowest energy vertical transition. The HOMO is distributed throughout the indolizine heterocycle as well as the squaraine core. However, negligible HOMO contribution is seen on the phenyl ring at the 2 position of the indolizine donor due to the large (~57°) dihedral angle between the phenyl group and the indolizine heterocycle causing a significant reduction in conjugation.[19] The auxiliary DMA donors on **1DMASQ**, **7DMASQ**, and **1,7DMASQ** are observed to have a portion of the HOMO delocalization across them and thus contribute to the HOMO of the fluorophores (Figure 3, Table S1). Like the HOMO, the LUMO of the fluorophores exhibits orbital distribution across the indolizine heterocycles and the squaraine core, however, there is negligible LUMO distribution on the auxiliary DMA groups.

Vertical transitions of the squaraine dyes were also assessed at the B3LYP[20]/6-311G(*d*,*p*)[21] level of theory with dichloromethane (DCM) as an implicit solvent with Gaussian16.[22] The following trend in vertical transition is observed for the squaraine derivatives: **2PhSQ** < **1PhSQ** < **1DMASQ** < **7DMASQ** < **1,7DMASQ** (Table S1). Addition of the DMA groups is observed to induce a bathochromic shift in the predicted absorption of the dyes, with the DMA group at the 7-position having a larger impact than the DMA group at the 1-position

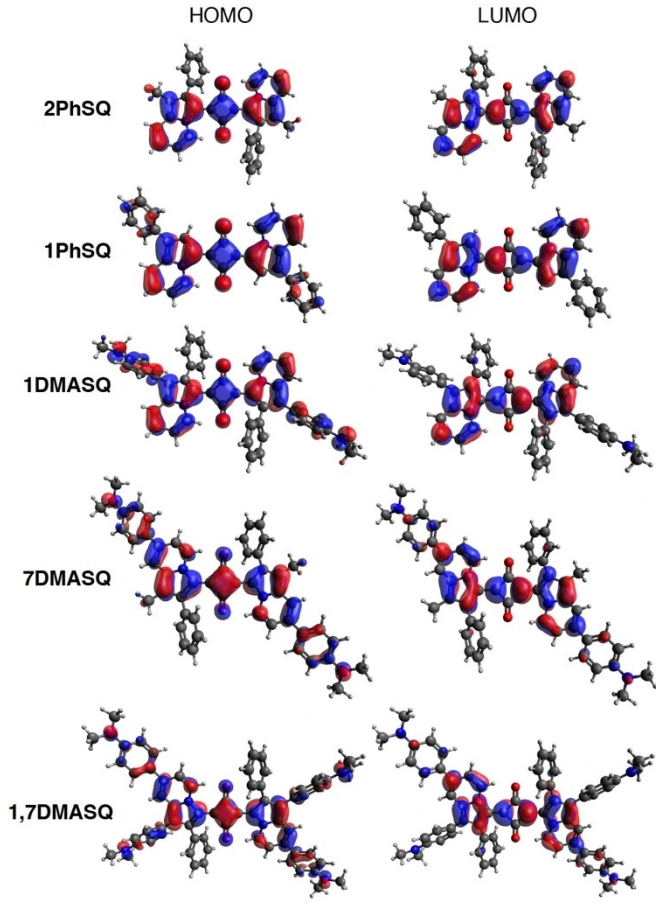

Figure 3. HOMO-LUMO orbitals of **2PhSQ**, **1PhSQ**, **1DMASQ**, **7DMASQ**, and **1,7DMASQ**.

(723 versus 711 nm for **7DMASQ** and **1DMASQ**, respectively). Addition of DMA groups at both the 1- and 7-position of **1,7DMASQ** is observed to have an additive effect, with a predicted vertical transition of 772 nm (Table S1). Removal of the phenyl group at the 2-position in **2PhSQ** and addition of a phenyl group to the 1-position in **1PhSQ** is observed to have a minor effect on the vertical transition of the dyes (629 nm for **2PhSQ** and 638 nm for **1PhSQ**); however, a notable increase in oscillator strength is observed (1.03 for **2PhSQ** and 1.45 for **1PhSQ**), likely due to the increased planarity of **1PhSQ** allowing for greater orbital overlap. The dihedral angle between the squaraine ring and indolizine heterocycle for the geometry optimized structures is 15° for **2PhSQ** and 1° for **1PhSQ**.

Synthesis

The novel indolizine squaraine derivatives synthesized herein were accessed *via* condensation of the indolizine donors with squaric acid (Scheme 1), as is typical for squaraine fluorophores. Yields for this step ranged from 32 to 63%. The indolizine donors used in the synthesis (**1**, **2**, **3**, **4**, see Figure S4 for structures) and the squaraine dyes, **2PhSQ** and **SO_3SQ**, were synthesized according to literature procedures.[16a,18–19,23]

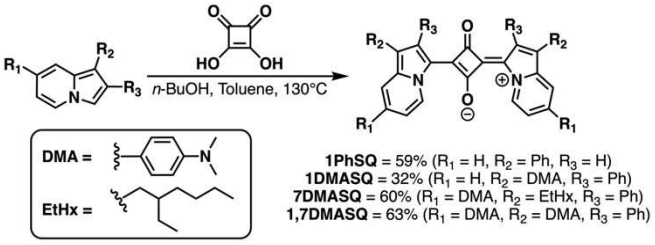

Scheme 1. Synthesis of **1PhSQ**, **1DMASQ**, **7DMASQ**, and **1,7DMASQ** fluorophores.

Photophysical Properties

With the newly synthesized dyes in hand, the photophysical properties including steady-state absorption and emission were investigated and compared. First, the absorption spectra of the squaraine dyes were taken in both dichloromethane (DCM) and tetrahydrofuran (THF) solutions to probe the photophysical properties in two aprotic solvents (Figure 4 and S1, Table 1). **1PhSQ** and **2PhSQ** demonstrated identical absorption maxima (λ_{abs}) in DCM (716 nm) and nearly identical λ_{abs} in THF (718 and 719 nm for **2PhSQ** and **1PhSQ**, respectively). The similarity in λ_{abs} of these two materials can be rationalized by the materials having similar electronics, conjugation lengths, and distribution of their frontier molecular orbitals, which exhibit minimal distribution on the phenyl ring whether at the 1- or 2-position

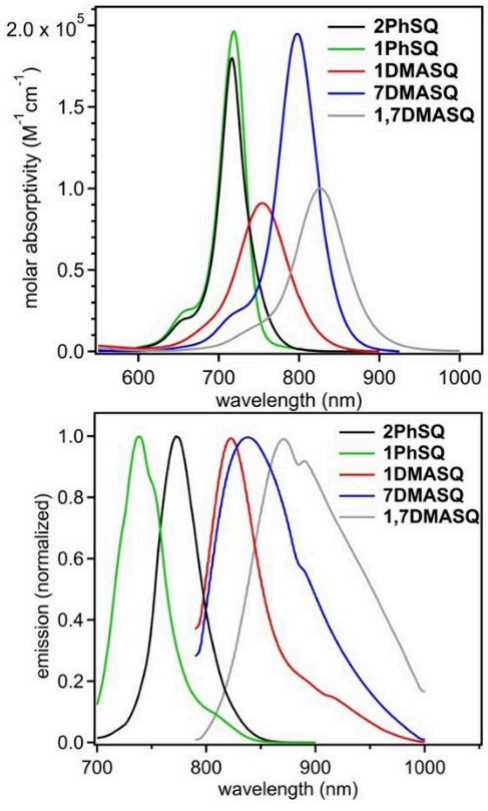

Figure 4. Molar absorptivity (top) and normalized emission (bottom) of **2PhSQ**, **1PhSQ**, **1DMASQ**, **7DMASQ**, and **1,7DMASQ** in DCM.

Table 1. Photophysical data of **1PhSQ**, **2PhSQ**, **1DMASQ**, **7DMASQ**, **1,7DMASQ**, **SO_3SQ** and **C3**.

Dye	Solvent	λ_{abs} [nm]	λ_{emis} [nm]	ε [$M^{-1}cm^{-1}$]	Stokes Shift [nm | eV]	Φ_F [%]	MB[a] [$M^{-1}cm^{-1}$]
1PhSQ	DCM	716	740	196,000	24 | 0.06	39.5	77,400
	THF	719	745	–	26 | 0.06	72.0	–
	Gly	722	740	–	18 | 0.04	30.3	–
2PhSQ	DCM	716	770	181,000	54 | 0.12	0.7	1,270
	THF	718	764	–	46 | 0.10	2.4	–
	Gly	714	731	–	17 | 0.04	37.1	–
1DMASQ	DCM	754	826	91,000	72 | 0.14	0.2	182
	THF	754	828	–	74 | 0.15	0.4	–
7DMASQ	DCM	798	840	195,000	42 | 0.08	2.7	5,270
	THF	798	846	–	48 | 0.09	3.1	–
	Gly [50%]	796	815	–	19 | 0.04	10.7	–
1,7DMASQ	DCM	827	872	100,000	45 | 0.08	1.0	1,000
	THF	827	881	–	54 | 0.09	3.9	–
SO_3SQ[b]	DMSO	720	734	145,000	14 | 0.03	8.6	12,500
	Gly	713	730	–	17 | 0.04	42.2	–
C3[b]	DCM	708	741	204,000	33 | 0.08	<1.0	$\leq 2{,}000$
	Gly	705	724	–	19 | 0.05	12.8	–

[a] MB = molecular brightness, calculated as the product of ε and Φ_F [b] Data for **SO_3SQ**[16a] in DMSO, and **C3**[24] in DCM are from the literature.

for **1PhSQ** and **2PhSQ**, respectively (Figure 3). TD-DFT predicts a higher ε for 1PhSQ compared to 2PhSQ, with oscillator strengths of 1.45 versus 1.03, respectively. This observation is confirmed experimentally as **1PhSQ** exhibits a slightly higher ε of 196,000 $M^{-1}cm^{-1}$ compared to **2PhSQ** at 181,000 $M^{-1}cm^{-1}$. The DMA substituted squaraines, **1DMASQ**, **7DMASQ**, and **1,7DMASQ** exhibit longer wavelength λ_{abs} compared to **2PhSQ** and **1PhSQ** as predicted computationally and as expected from adding additional electron rich groups to the indolizine donors. **1DMASQ**, employing the DMA donor at the 1-position, has a λ_{abs} of 754 nm in DCM, a 38 nm (0.09 eV) bathochromic shift compared to **2PhSQ**. However, ε of **2PhSQ** is nearly double that of **1DMASQ** presumably due to the steric interaction of the DMA at the 1-position and the phenyl group at the 2-position of the indolizine donor. **7DMASQ**, employing the DMA donor at the 7-position, has a λ_{abs} of 798 nm in DCM, an 82 nm (0.18 eV) bathochromic shift compared to **2PhSQ**. Further, **7DMASQ** also has a higher ε than **2PhSQ** at 195,000 $M^{-1}cm^{-1}$, which is comparable to that of **1PhSQ**. In comparing the two dyes with a single auxiliary DMA donor, substitution at the 7-position versus the 1-position yields a bathochromic shift of 44 nm (0.09 eV) along with a doubling in ε. **1,7DMASQ**, employing DMA donors at both the 1- and 7-positions, has a λ_{abs} of 827 nm in DCM, a 111 nm (0.23 eV) bathochromic shift compared to **2PhSQ**, and 29 nm (0.05 eV) compared to **7DMASQ**. However, due to the presence of the DMA group at the 1-position of the indolizine donor, **1,7DMASQ** suffers from a decrease in ε (100,000 $M^{-1}cm^{-1}$) as **1DMASQ**. Similar trends are observed in THF (Figure S1, Table 1).

Steady-state fluorescence spectroscopy was conducted to determine the λ_{emis}, Φ_F, and Stokes shift of the fluorophores (Figure 4 and S1, Table 1). The Stokes shift is of concern since it reveals information about the molecular reorganization between the ground state and excited state geometries of the fluorophores, a metric that is important for viscosity sensitivity. **2PhSQ** exhibits a λ_{emis} of 770 nm in DCM with a Stokes shift of 54 nm (0.12 eV). **1PhSQ** is observed to emit at higher energies compared to **2PhSQ** with a λ_{emis} of 740 nm in DCM and a Stokes shift of 24 nm (0.06 eV). The halving of the Stokes shift of **1PhSQ** compared to **2PhSQ** indicates a smaller degree of reorganization between the ground and excited state geometries of the fluorophore. The fluorophores containing auxiliary DMA donors all demonstrate lower energy λ_{emis} compared to **2PhSQ**, with λ_{emis} of 826, 840, and 872 nm in DCM for **1DMASQ**, **7DMASQ**, and **1,7DMASQ**, respectively. The Stokes shift of the dyes containing the auxiliary DMA donors is observed to be 72 nm (0.14 eV), 42 nm (0.08 eV), and 45 nm (0.08 eV) for **1DMASQ**, **7DMASQ**, and **1,7DMASQ**, respectively.

Φ_F of the fluorophores were determined to understand the effect of structural modification on fluorescence intensity of the materials. All of the dyes were observed to have a greater Φ_F in THF compared to DCM, with increases ranging from ~1.2 to ~3.9 times higher. **2PhSQ** exhibited a Φ_F of 0.7% in DCM and 2.4% in THF, which is comparable to the previously reported value of 3.7% in toluene. However, a simple shift of the phenyl ring from the 2-postion to the 1-position for **1PhSQ** yielded a remarkable increase in the Φ_F to 39.5% in DCM and 72.0% in THF (Table 1). A 72.0% Φ_F from a NIR fluorophore is exceptional. The higher Φ_F of **1PhSQ** relative to **2PhSQ** is likely linked to the decrease in the Stokes shift of **1PhSQ** compared to **2PhSQ**, which indicates similar ground state and excited state geometries and a higher probability for radiative decay. **1DMASQ** exhibits the smallest Φ_F of the series at 0.2% in DCM and 0.4% in THF, which is likely due to the significant steric interactions of the 2 phenyl group and 1 DMA group promoting non-radiative relaxation pathways. **7DMASQ** has a Φ_F slightly higher than that of **2PhSQ** (2.7 versus 0.7% in DCM and 3.1 versus 2.4% in THF, respectively). Given the lower energy emission of

7DMASQ a lower Φ_F would be anticipated given the energy gap law.[25] **1,7DMASQ** is observed to have a Φ_F of 1.0% in DCM, and the second highest Φ_F of the series in THF at 3.9%. This is consistent with **1,7DMASQ** having a significantly smaller Stokes shift than **1DMASQ**. Molecular brightness (MB, defined $MB = \varepsilon \times \Phi_F$) is an important metric when comparing fluorophores intended for *in vivo* imaging applications since it accounts for both absorption and emission intensity. MB values in DCM were observed to be 1,270, 77,400, 182, 5,270, and 1,000 $M^{-1}cm^{-1}$ for **2PhSQ**, **1PhSQ**, **1DMASQ**, **7DMASQ**, and **1,7DMASQ**, generating a trend of **1PhSQ** > **7DMASQ** > **2PhSQ** > **1,7DMASQ** > **1DMASQ**. Notably, a molecular brightness of 77,400 $M^{-1}cm^{-1}$ is exceptionally high in the NIR region.

Electrochemical Properties

Cyclic voltammetry experiments were conducted with the indolizine squaraine dyes to determine how the energetics of the fluorophores vary based on the indolizine donor utilized. The ground state oxidation ($E_{S+/S}$) and reduction ($E_{S/S-}$) potentials of the dyes are reported in Figures 5 & S2 and Table S2. The trend in $E_{S+/S}$ (from least negative to most negative) was observed to be: **1PhSQ** < **2PhSQ** < **1DMASQ** < **7DMASQ** < **1,7DMASQ** (Figure 5). The $E_{S+/S}$ values demonstrate that as the electron density of the donor increases, $E_{S+/S}$ becomes more negative, indicating an increase in the energy of the HOMO with a tunable range of near 500 mV. Unlike $E_{S+/S}$, $E_{S/S-}$ of the dyes demonstrated no obvious trend and was more closely grouped energetically (260 mV variation). The excited state oxidation potentials ($E_{S+/S*}$) were determined via the equation: $E_{S+/S*} = E_{S+/S} - E_g^{opt}$ (where E_g^{opt} is determined from the absorption onset in DCM solution) and were observed to follow the same trend as $E_{S/S-}$ again with a small variation (< 200 mV). While $E_{S+/S*}$ and $E_{S/S-}$ are not the same value, they both provide information about the LUMO of the fluorophore and indicate that the indolizine donors are having modest effects on the LUMO energies.

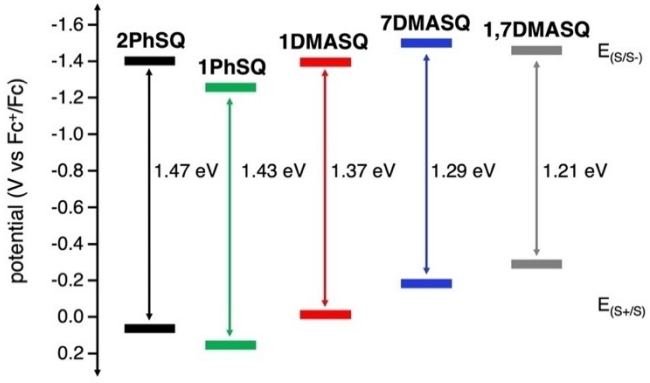

Figure 5. Experimentally determined ground state oxidation and reduction potentials of **1PhSQ**, **2PhSQ**, **1DMASQ**, **7DMASQ**, and **1,7DMASQ** in DCM solution with a 0.1 M NBu_4PF_6 electrolyte, glassy carbon working electrode, Ag pseudo reference electrode, and Pt counter electrode. Potentials are referenced to Fc^+/Fc at 0.00 V.

Fluorescence Lifetimes

Photoluminescent (PL) lifetimes of the squaraine dyes are studied herein in DCM solution along with an indolizine cyanine dye, **C3** (Table 2 and S3, Figure 6 and S3). **1PhSQ** was observed to have the longest PL lifetime of the series at 2131 ps. The longer excited state lifetime of **1PhSQ** is likely due to the increased planarity of the molecule, which maximizes radiative decay of the excited state and minimizes the rapid nonradiative processes (Figure 6, Table 2). The long PL lifetime of **1PhSQ** is also reflected in it having the highest Φ_F of the series since PL lifetimes are known to be related to the Φ_F of fluorophores.[26] On the other hand, **2PhSQ** exhibits a shorter PL lifetime of < 60 ps (noted as less than due to limitations of the instrument response function). This also coincides with **2PhSQ** having a much smaller Φ_F than **1PhSQ**. **1DMASQ** also demonstrates a PL lifetime near the instrument response function at just 68 ps, indicating rapid nonradiative decay processes that also coincide with it having the smallest Φ_F of the series. **7DMASQ** and **1,7DMASQ** demonstrate appreciable PL lifetimes of 371 and 123 ps, respectively. Both dyes also exhibit appreciable Φ_F at 3.1% and 3.9% for **7DMASQ** and **1,7DMASQ**, respectively. The overall trend in PL lifetimes is as follows: **2PhSQ** ≃ **1DMASQ** < **1,7DMASQ** < **7DMASQ** ≪ **1PhSQ**. **SO_3SQ**, which shows dramatically increased fluorescence quantum yields in confined environments as previous reported, displays a PL lifetime of 211 ps in water.[16b] This is comparable to other water soluble NIR squaraines.[27] The fluorescent lifetime of the indolizine cyanine dye, **C3**, used herein to allow for comparison of a cyanine and

Table 2. Photoluminescent lifetime and fluorescent quantum yield data of the dyes in DCM solution, except for **SO_3SQ** which was studied in H_2O.

Dye	Rate [1/ps]	Lifetime [ps]	Φ_F (%)
1PhSQ	0.0005	2131	39.5
2PhSQ	> 0.017	< 60	0.7
1DMASQ	0.0147	68	0.2
7DMASQ	0.0027	371	2.7
1,7DMASQ	0.0081	123	1.0
SO_3SQ	0.0047	211	0.8[a]
C3	> 0.017	< 60	< 1.0[a]

[a] Literature values for **SO_3SQ** and **C3** respectively.[16a,24]

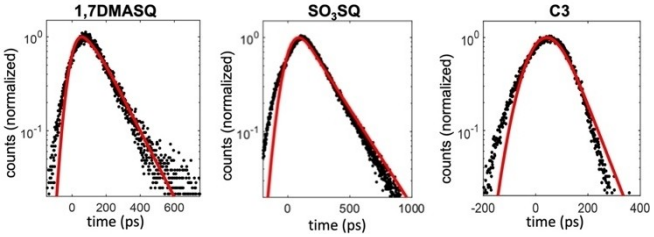

Figure 6. Photoluminescent lifetime graphs of the dyes in DCM solution, except for **SO_3SQ** which was studied in H_2O. The lifetime of 2PhSQ is less than the instrument response function.

squaraine bridge, (see Figure S4 for structure) was also measured and observed to be less than the response function of the instrument which similarly coincides with it having a low Φ_F of $< 1.0\,\%$.[28]

Viscosity Sensitivity

Select molecules are known to exhibit significant variation in their photophysical properties depending on their local molecular environment (Table S4). Variables such as temperature,[29] solvent dielectric constant,[24] and hydrogen bonding capabilities[30] are frequently studied for their impact on photophysical properties. Solvent viscosity is a less frequently investigated variable that has the capacity to greatly affect the molecular brightness of many fluorophores.[31] Fluorophores that exhibit strong viscosity responses are of particular interest to fluorescence biological imaging due to the high local viscosity of tissues and intracellular environments. Thus, fluorophores that exhibit a strong viscosity response would "light-up" in a highly viscous biological matrix, improving their MB and utility as *in vivo* imaging fluorophores. This was previously observed with the indolizine squaraine, **SO_3SQ**, as it was observed to exhibit a Φ_F of 64.9 % in human serum,[16b] a record for the spectral region, but a Φ_F of only 0.3 % in aqueous solvent.[16a] Current understanding of viscosity-sensitive fluorophores links a high degree of molecular rotation to a strong viscosity response.[31] This suggests that in low viscosity environments, excited states more easily decay *via* nonradiative pathways due to easily accessible rotations and vibrations. Conversely, in high viscosity environments, excited states more easily decay *via* radiative pathways such as fluorescence due to the restriction of molecular motion.[32] In highly viscous environments, nonradiative relaxation pathways stemming from intramolecular motion are suppressed due to increased rigidity of the fluorophore within the viscous solvent matrix. In fluorophores exhibiting viscosity sensitivity, there is typically a linear relationship between the viscosity of the solution (η) and Φ_F. This relationship is commonly represented as log(η) versus log(Φ_F) to more clearly show the linearity of the relationship by expanding the respective axes, and is referred to as the Forster-Hoffmann plot.[33] Herein, the viscosity response of the indolizine squaraine molecular scaffold is probed to investigate the mechanism of this previously observed fluorescence "switch-on" behavior.

2PhSQ was subjected to viscosity studies by collecting the absorption and fluorescence emission spectra in different ratios of methanol (MeOH) and glycerol solutions to determine the viscosity sensitivity of the fluorophore (Figures 7 and S5, Table 3).[10,34] The absorption spectrum of **2PhSQ** is observed to gradually decrease in intensity and shift towards lower energy as the viscosity of the solution increases from 100 % MeOH to 100 % glycerol. The emission spectrum of **2PhSQ** demonstrates a substantial increase in fluorescence intensity and consequently a dramatic increase in Φ_F from a mere 0.3 % in MeOH (low viscosity) to 37.1 % in glycerol (high viscosity). The Forster-Hoffman plot is generated by plotting the log(η) versus log(Φ_F)

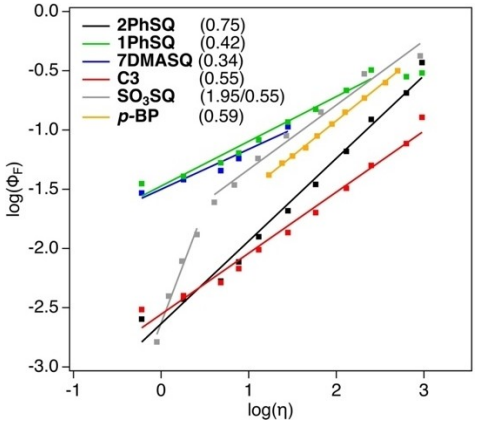

Figure 7. Forster-Hoffman plot and Forster-Hoffman slopes (value in parentheses next to dye code) for **2PhSQ**, **1PhSQ**, **7DMASQ**, **C3**, ***p*-BP** in MeOH/glycerol, and **SO_3SQ** in H_2O/glycerol mixtures. Experimental data presented herein has been reproduced on separate instruments and is accurate to slopes of ± 0.01.

Table 3. Φ_F[JHD1] of **2PhSQ**, **1PhSQ**, **SO_3SQ**, **7DMASQ**, and **C3** in MeOH/glycerol mixtures increasing fractions of glycerol.

Glycerol [%]	1PhSQ Φ_F [%]	2PhSQ Φ_F [%]	7DMASQ Φ_F [%]	SO_3SQ Φ_F[a] [%]	C3 Φ_F [%]
0	3.5	0.3	2.9	0.2	0.3
10	4.1	0.4	3.8	0.4	0.4
20	5.3	0.5	4.5	0.8	0.5
30	6.4	0.8	5.7	1.3	0.7
40	8.3	1.3	8.2	2.5	1.0
50	11.7	2.1	10.7	3.4	1.4
60	14.9	3.5	–	5.8	2.0
70	21.6	6.6	–	8.9	3.2
80	32.1	12.3	–	14.2	5.0
90	28.2	20.5	–	29.8	7.7
100	30.3	37.1	–	42.2	12.8

[a] Φ_F data obtained in volume percent of H_2O/glycerol mixtures.

to yield a linear relationship that reveals the relative viscosity sensitivities of the material (Figure 7). This process was repeated for other derivatives including **1PhSQ**, **C3**, and **7DMASQ** in MeOH/glycerol mixtures, as well as **SO_3SQ** in H_2O/glycerol mixtures, to compare the relative viscosity responses of the materials.

The slope of the line of best fit represents the viscosity sensitivity of the fluorophore. **2PhSQ** exhibits a slope of 0.75 which indicates a very high sensitivity to solution viscosity as the highly sensitive reference material, ***p*-BP**, exhibits a slope of 0.59.[10] From a brief search of the literature, a viscosity sensitivity of 0.75 appears to be an exceptional viscosity sensitivity amongst NIR fluorescent-based viscosity sensors.[5b,35] **1PhSQ** was observed to a have slope of 0.42 through the linear viscosity region. While this is a respectable value, it is much smaller than that of **2PhSQ**. **7DMASQ** exhibits a viscosity sensitivity of 0.34, indicating moderate viscosity sensitivity. Further, **7DMASQ** was only studied in MeOH/glycerol mixtures of up to 50 % glycerol as higher ratios of the viscous solvent induced dye aggregation as seen by broadening in the

absorption curves and the absence of detectable emission signal. This is likely due to the two large aliphatic chains of **7DMASQ** causing the dye to preferentially aggregate at higher ratios of glycerol. Regardless, enough data points were gathered to exhibit a linear relationship within the plot and determine the viscosity sensitivity of the material. **1DMASQ** and **1,7DMASQ** were not analyzed due to substantially lower solubilities of these dyes relative to **7DMASQ**, which is already challenging to measure the viscosity sensitivity of due to solubility. **C3** and **C5**, a trimethine and pentamethine indolizine cyanine dye, respectively (structures given in Figure S4), were also tested for viscosity sensitivity to explore if the cyanine scaffold exhibits viscosity sensitivity similar to the squaraine scaffold. Preliminary experiments demonstrated little to no viscosity sensitivity for **C5** (Figure S5), which showed minimal change in fluorescence intensity based on solvent viscosity. However, **C3** was observed to exhibit reasonable viscosity sensitivity in preliminary experiments and was studied further. A Forster-Hoffmann plot was generated for **C3**, generating a line of best fit with a slope of 0.55 (Figure 7, Figure S5, Table 3). This value is lower than that of **2PhSQ**, indicating a lower viscosity sensitivity for the cyanine dye than the squaraine dye, however, it is comparable to high performing literature standards like ***p*-BP**. The higher sensitivity of **C3** relative to **C5** is presumably due to the increased steric interaction of the indolizines of **C3** as previously shown in the literature.[24] The following trend in Forster-Hoffman values was observed herein **2PhSQ** > ***p*-BP** > **C3** > **1PhSQ** > **7DMASQ** > **C5**.

The high viscosity response of **2PhSQ** could be used to rationalize the remarkably high fluorescence response of **SO_3SQ** when bound to serum albumin, which is presumably due to the high local viscosity of the Heme cleft where the dye is predicted to bind.[16a] To probe this theory, the viscosity sensitivity of **SO_3SQ** was studied in H_2O/glycerol mixtures (Figure 7 and S5, Table 3). Contrary to **2PhSQ**, the absorbance of **SO_3SQ** increases as the ratio of glycerol increases, nearly doubling from ~0.6 to ~1.2. The absorbance is also observed to shift towards lower energy as the percent volume of glycerol increases. The emission intensity of **SO_3SQ** is observed to increase dramatically as the percent volume of glycerol increases, depicting strong viscosity sensitivity for the material. Φ_F is observed to increase from a 0.2% in water to 42.2% in glycerol. The Forster-Hoffmann plot of **SO_3SQ** is observed to have roughly two regions of linearity. The first region spans from 0 to 30% glycerol and exhibits a slope of 1.95 which is exceptionally high and shows a strong dependence on solvent viscosity but may be significantly affected by dye aggregation reduction with more organic solvent rather than due to viscosity alone as indicated by the absorption curve changes. The second region spans from 40 to 100% glycerol and demonstrates a slope of 0.55, which is still comparable to both ***p*-BP** and **C3**. Overall, **SO_3SQ** is observed to demonstrate a high sensitivity to solvent viscosity which rationalizes its exceptional Φ_F in serum solutions.

It has previously been shown that viscosity sensitivity originates from a fluorophore having a nonradiative excited state geometry that is rotationally accessible in low viscosity solvents, but not high viscosity solvents.[10] The magnitude of viscosity sensitivity of the fluorophore is governed by the rotational energy barrier required to access this non-radiative excited state geometry being environment dependent. In a high viscosity environment, the rotational barrier should be high which prohibits accessing the non-radiative state. However, in a low viscosity environment the rotational barrier needs to be sufficiently low to allow for the fluorophore to readily access the non-radiative state. The difference in energy of the rotational barrier for these two environments determines the viscosity sensitivity of the system provided both a trapped radiative state (high viscosity) and an accessible non-radiative state (low viscosity) can be accessed. While the magnitude of viscosity sensitivity is difficult to predict for a given fluorophore's chemical structure, the incorporation of rotatable groups within the π-system is of paramount importance to impart viscosity sensitivity in a fluorophore.[9a–d,f,36]

To rationalize the high viscosity sensitivity of the **2PhSQ** scaffold relative to the other squaraine fluorophores tested herein, the rotational barriers at the indolizine-squaraine core were probed for the ground and excited state geometries of **2PhSQ** and **1PhSQ** (Figure S6 and 8). The ground and excited state geometries of the fluorophores were observed to have nearly degenerate energy profiles (Figure 8). Previous studies with indolizine squaraines containing the aryl groups at the 2-position demonstrated that cis/trans isomerization is slow for larger groups at room temperature, which is corroborated with the data given herein illustrating that the energy available at room temperature is near the 0° energy barrier for rotation.[19] This also suggests that **1PhSQ** should be able to rotate rapidly between the cis and trans conformers at room temperature since the 0° energy barrier is small. The edges of the graph near 180° and −180° demonstrate that **1PhSQ** has a higher energy barrier to rotation that **2PhSQ**, with energy barriers of ~45 and 30 kcal/mol, respectively. This indicates that at the excitation wavelengths used herein, where 770 nm is equivalent to

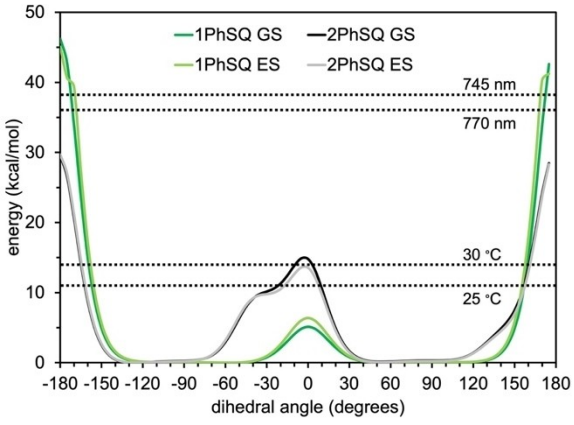

Figure 8. Relative energy versus dihedral angle plot for the ground and excited state geometries for **1PhSQ** and **2PhSQ**. Ground state geometries are shown as the darker colors and excited state geometries are the lighter colors. 0° represents the trans geometry with respect to the indolizine heterocycles to each other, and 180° represents the cis geometry. The dotted lines represent the amount of available energy (in kcal/mol) at the respective temperatures or wavelengths listed next to them.

~36 kcal/mol, there is sufficient energy to overcome the 180° energy barrier for **2PhSQ**, but not **1PhSQ**. The 180° geometry may present a nonradiative relaxation pathway conformation that is available for **2PhSQ** but not **1PhSQ**. The available nonradiative relaxation pathway could result in the low Φ_F of **2PhSQ** in low viscosity solvents as the molecule is able to easily rotate through this barrier; however, high viscosity solvents restrict motion and thus increase the relative energy of this barrier and do not allow access to it, resulting in a substantial increase in Φ_F. This rationalizes the much higher slope in the Forster-Hoffman plot observed for **2PhSQ** compared to **1PhSQ**, which cannot rotate freely regardless of solvent viscosity. The lower slope observed for **7DMASQ** could be due to the large 2-ethylhexyl chain increasing the relative energy barrier and rate of rotation by acting as an anchor and needing to be "drug" through the solvent, resulting in a similarly lower slope in the Forster-Hoffman plot like **1PhSQ**.

Conclusions

Four new NIR emissive indolizine squaraine dyes were synthesized, three of which were decorated with auxiliary DMA donors at carbons 1 and 7 on the indolizine heterocycle. Computational analysis guided the dye design and revealed significant contribution of the DMA groups to the HOMO, which was observed experimentally as bathochromic shifts in the absorption and emission of the DMA containing dyes. The dyes were observed to absorb and emit in the NIR region, with absorption maxima ranging from 719 to 827 nm and emission maxima ranging from 748 to 881 nm. One of the highest Φ_F in the NIR of 72% has been realized for **1PhSQ** in THF solution. Viscosity sensitivity studies show that **2PhSQ** is one of the highest NIR viscosity sensors to date with a slope of 0.75 in the Forster-Hoffman plot. This could be useful for monitoring changes in the intracellular environment and also rationalizes the "switch-on" fluorescence response of previously studied **SO_3SQ**. Thus, this work further implicates indolizine squaraine fluorophores as practical *in vivo* fluorescence imaging dyes and intracellular viscosity sensors.

Supporting Information

The supporting information containing supplementary graphs and tables is available as a separate document. The authors have cited additional references within the Supporting Information (Ref. [9–10, 21, 22b, 24, 37])

Acknowledgements

DN, CS, WEM, MM, NIH and JHD acknowledge NSF OIA-1757220 for support of this work. MM, JHD, and NIH thank NSF REU CHE-1757888 for supporting this work. This material is based upon work supported by the National Science Foundation Graduate Research Fellowship Program awarded to WEM. Any opinions, findings, and conclusions or recommendations expressed in this material are those of the author(s) and do not necessarily reflect the views of the National Science Foundation.

Conflict of Interests

The authors declare no conflict of interest.

Data Availability Statement

The data that support the findings of this study are available from the corresponding author upon reasonable request.

Keywords: squaraine · near infrared · viscosity sensor · fluorophore · indolizine

[1] P. Strzyz, *Nat. Rev. Mol. Cell Biol.* **2023**, *24*, 3.
[2] P. Mecocci, M. F. Beal, R. Cecchetti, M. C. Polidori, A. Cherubini, F. Chionne, L. Avellini, G. Romano, U. Senin, *Mol. Chem. Neuropathol.* **1997**, *31*, 53–64.
[3] A. Perazzo, Z. Peng, Y.-N. Young, Z. Feng, D. K. Wood, J. M. Higgins, H. A. Stone, *Soft Matter* **2022**, *18*, 554–565.
[4] J. Eckmann, S. H. Eckert, K. Leuner, W. E. Muller, G. P. Eckert, *Int. J. Biochem. Cell Biol.* **2013**, *45*, 76–80.
[5] a) Y. Zhang, X. Yue, B. Kim, S. Yao, K. D. Belfield, *Chem. Eur. J.* **2014**, *20*, 7249–7253; b) H. Xiao, P. Li, B. Tang, *Chem. Eur. J.* **2021**, *27*, 6880–6898; c) K. S. Cunningham, A. I. Gotlieb, *Lab. Invest.* **2005**, *85*, 9–23.
[6] K. Bera, A. Kiepas, I. Godet, Y. Li, P. Mehta, B. Ifemembi, C. D. Paul, A. Sen, S. A. Serra, K. Stoletov, J. Tao, G. Shatkin, S. L. Lee, Y. Zhang, A. Boen, P. Mistriotis, D. M. Gilkes, J. D. Lewis, C.-M. Fan, A. P. Feinberg, M. A. Valverde, S. X. Sun, K. Konstantopoulos, *Nature* **2022**, *611*, 365–373.
[7] C. Ma, W. Sun, L. Xu, Y. Qian, J. Dai, G. Zhong, Y. Hou, J. Liu, B. Shen, *J. Mater. Chem. B* **2020**, *8*, 9642–9651.
[8] M. A. Nour, S. M. Khan, N. Qaiser, S. A. Bunaiyan, M. M. Hussain, *Eng. Rep.* **2021**, *3*, 12315.
[9] a) X. Yuan, Y. Hu, K. Zheng, D. Liu, P. Su, C. Hu, J. Yan, N. Zhang, *J. Mol. Liq.* **2022**, *349*; b) K. Dou, W. Huang, Y. Xiang, S. Li, Z. Liu, *Anal. Chem.* **2020**, *92*, 4177–4181; c) X. Zhang, H. Yan, F. Huo, J. Chao, C. Yin, *Sens. Actuators B* **2021**, *344*; d) Y. Liu, X. Li, W. Shi, H. Ma, *Chem. Commun.* **2022**, *58*, 12815–12818; e) W. Du, J. Wang, H. Fang, W. Ji, Y. Liu, Y. Qu, D. Zhang, T. Shao, X. Hou, Q. Wu, *Sens. Actuators B* **2022**, *370*, 132456; f) L. Xu, Y. Huang, X. Peng, K. Wu, C. Huang, L. Liu, *Mater Adv* **2022**, *3*, 3545–3553.
[10] X. Liu, W. Chi, Q. Qiao, S. V. Kokate, E. P. Cabrera, Z. Xu, X. Liu, Y. T. Chang, *ACS Sens.* **2020**, *5*, 731–739.
[11] D. Su, C. L. Teoh, N. Gao, Q.-H. Xu, Y.-T. Chang, *Sensors* **2016**, *16*, 1397.
[12] L. Wang, Y. Xiao, W. Tian, L. Deng, *J. Am. Chem. Soc.* **2013**, *135*, 2903–2906.
[13] H. Dai, Q. Shen, J. Shao, W. Wang, F. Gao, X. Dong, *Innovation* **2021**, *2*, 100082.
[14] K. Ilina, W. M. MacCuaig, M. Laramie, J. N. Jeouty, L. R. McNally, M. Henary, *Bioconjugate Chem.* **2019**, *31*, 194–213.
[15] Y. Yadav, E. Owens, S. Nomura, T. Fukuda, Y. Baek, S. Kashiwagi, H. S. Choi, M. Henary, *J. Med. Chem.* **2020**, *63*, 9436–9445.
[16] a) W. E. Meador, S. A. Autry, R. N. Bessetti, J. N. Gayton, A. S. Flynt, N. I. Hammer, J. H. Delcamp, *J. Org. Chem.* **2020**, *85*, 4089–4095; b) W. E. Meador, K. Kapusta, I. Owolabi, S. A. Autry, J. Saloni, W. Kolodziejczyk, N. I. Hammer, A. S. Flynt, G. A. Hill, J. H. Delcamp, *ChemPhotoChem* **2022**, *6*.
[17] a) J. Watson, R. R. Rodrigues, J. H. Delcamp, *Cell Rep. Phys. Sci.* **2022**, *3*; b) S. Galliano, V. Novelli, N. Barbero, A. Smarra, G. Viscardi, R. Borrelli, F. Sauvage, C. Barolo, *Energies* **2016**, *9*, 486.
[18] D. Ndaleh, C. Smith, M. Loku Yaddehige, A. K. Shaik, D. L. Watkins, N. I. Hammer, J. H. Delcamp, *J. Org. Chem.* **2021**, *86*, 15376–15386.

[19] L. E. McNamara, T. A. Rill, A. J. Huckaba, V. Ganeshraj, J. Gayton, R. A. Nelson, E. A. Sharpe, A. Dass, N. I. Hammer, J. H. Delcamp, *Chem. Eur. J.* **2017**, *23*, 12494–12501.
[20] a) A. Becke, *J. Chem. Phys.* **1993**, *98*, 5648–5652; b) P. J. Stephens, F. J. Devlin, C. F. Chabalowski, M. J. Frisch, *J. Phys. Chem.* **1994**, *98*, 11623–11627.
[21] a) M. J. Frisch, J. A. Pople, J. S. Binkley, *J. Chem. Phys.* **1984**, *80*, 3265–3269; b) C. Lee, W. Yang, R. G. Parr, *Phys. Rev. B: Condens. Matter Mater. Phys.* **1988**, *37*, 785–789.
[22] M. J. Frisch, G. W. Trucks, H. B. Schlegel, G. E. Scuseria, M. A. Robb, J. R. Cheeseman, G. Scalmani, V. Barone, G. A. Petersson, H. Nakatsuji, X. Li, M. Caricato, A. V. Marenich, J. Bloino, B. G. Janesko, R. Gomperts, B. Mennucci, H. P. Hratchian, J. V. Ortiz, A. F. Izmaylov, J. L. Sonnenberg, D. Williams-Young, F. Ding, F. Lipparini, F. Egidi, J. Goings, B. Peng, A. Petrone, T. Henderson, D. Ranasinghe, V. G. Zakrzewski, J. Gao, N. Rega, G. Zheng, W. Liang, M. Hada, M. Ehara, K. Toyota, R. Fukuda, J. Hasegawa, M. Ishida, T. Nakajima, Y. Honda, O. Kitao, H. Nakai, T. Vreven, K. Throssell, J. A. Montgomery, Jr., J. E. Peralta, F. Ogliaro, M. J. Bearpark, J. J. Heyd, E. N. Brothers, K. N. Kudin, V. N. Staroverov, T. A. Keith, R. Kobayashi, J. Normand, K. Raghavachari, A. P. Rendell, J. C. Burant, S. S. Iyengar, J. Tomasi, M. Cossi, J. M. Millam, M. Klene, C. Adamo, R. Cammi, J. W. Ochterski, R. L. Martin, K. Morokuma, O. Farkas, J. B. Foresman, and D. J. Fox, *Gaussian 16*, *Rev. C.01*, Wallingford, CT, **2016**.
[23] E. Pohjala, *Tetrahedron Lett.* **1972**, *13*, 2585–2588.
[24] J. Gayton, S. A. Autry, W. Meador, S. R. Parkin, G. A. Hill Jr, N. I. Hammer, J. H. Delcamp, *J. Org. Chem.* **2018**, *84*, 687–697.
[25] a) R. Englman, J. Jortner, *Mol. Phys.* **1970**, *18*, 145–164; b) W. Siebrand, *J. Chem. Phys.* **1967**, *47*, 2411–2422; c) J. V. Caspar, B. P. Sullivan, E. M. Kober, T. J. Meyer, *Chem. Phys. Lett.* **1982**, *91*, 91–95; d) H. C. Friedman, E. D. Cosco, T. L. Atallah, S. Jia, E. M. Sletten, J. R. Caram, *Chem* **2021**, *7*, 3359–3376.
[26] a) E. D. Cosco, B. A. Arús, A. L. Spearman, T. L. Atallah, I. Lim, O. S. Leland, J. R. Caram, T. S. Bischof, O. T. Bruns, E. M. Sletten, *J. Am. Chem. Soc.* **2021**, *143*, 6836–6846; b) M. Pengshung, P. Neal, T. L. Atallah, J. Kwon, J. R. Caram, S. A. Lopez, E. M. Sletten, *Chem. Commun.* **2020**, *56*, 6110–6113.
[27] A. L. Tatarets, I. A. Fedyunyayeva, T. S. Dyubko, Y. A. Povrozin, A. O. Doroshenko, E. A. Terpetschnig, L. D. Patsenker, *Anal. Chim. Acta* **2006**, *570*, 214–223.
[28] M. Wang, Y. Zhang, X. Yue, S. Yao, M. V. Bondar, K. D. Belfield, *Molecules* **2016**, *21*, 709.
[29] a) A. Vysniauskas, B. Cornell, P. S. Sherin, K. Maleckaite, M. Kubankova, M. A. Izquierdo, T. T. Vu, Y. A. Volkova, E. M. Budynina, C. Molteni, *ACS Sens.* **2021**, *6*, 2158–2167; b) A. Vyšniauskas, M. Qurashi, N. Gallop, M. Balaz, H. L. Anderson, M. K. Kuimova, *Chem. Sci.* **2015**, *6*, 5773–5778.
[30] M.-Y. Wu, K. Li, Y.-H. Liu, K.-K. Yu, Y.-M. Xie, X.-D. Zhou, X.-Q. Yu, *Biomaterials* **2015**, *53*, 669–678.
[31] J. Sutharsan, D. Lichlyter, N. E. Wright, M. Dakanali, M. A. Haidekker, E. A. Theodorakis, *Tetrahedron* **2010**, *66*, 2582–2588.
[32] M.-X. Hou, L.-Y. Liu, K.-N. Wang, X.-J. Chao, R.-X. Liu, Z.-W. Mao, *New J. Chem.* **2020**, *44*, 11342–11348.
[33] T. Förster, G. Hoffmann, *Z. Phys. Chem.* **1971**, *75*, 63–76.
[34] J. A. Levitt, P. H. Chung, M. K. Kuimova, G. Yahioglu, Y. Wang, J. Qu, K. Suhling, *ChemPhysChem* **2011**, *12*, 662–672.
[35] X. Liu, W. Chi, Q. Qiao, S. V. Kokate, E. P. Cabrera, Z. Xu, X. Liu, Y.-T. Chang, *ACS Sens.* **2020**, *5*, 731–739.
[36] J. Liu, W. Zhang, C. Zhou, M. Li, X. Wang, W. Zhang, Z. Liu, L. Wu, T. D. James, P. Li, B. Tang, *J. Am. Chem. Soc.* **2022**, *144*, 13586–13599.
[37] a) K. Rurack, M. Spieles, *Anal. Chem.* **2011**, *83*, 1232–1242; b) A. Becke, *J. Chem. Phys.* **1993**, *98*, 5648; c) M. M. Francl, W. J. Pietro, W. J. Hehre, J. S. Binkley, M. S. Gordon, D. J. DeFrees, J. A. Pople, *J. Chem. Phys.* **1982**, *77*, 3654–3665; d) W. J. Hehre, R. Ditchfield, J. A. Pople, *J. Chem. Phys.* **1972**, *56*, 2257–2261; e) J. Liu, W. Zhang, C. Zhou, M. Li, X. Wang, W. Zhang, Z. Liu, L. Wu, T. D. James, P. Li, *J. Am. Chem. Soc.* **2022**, *144*, 13586–13599.

Manuscript received: September 8, 2023
Revised manuscript received: December 14, 2023
Accepted manuscript online: December 15, 2023
Version of record online: January 23, 2024